Article

Discovery Medicine 2023; 35(176): 251–263
https://doi.org/10.24976/Discov.Med.202335176.26

Curcumin Induces Ferroptosis in A549 CD133$^+$ Cells through the GSH-GPX4 and FSP1-CoQ10-NAPH Pathways

Jiajing Zhou[1,†], Lanyue Zhang[2,†], Jifeng Yan[3], Aihua Hou[1], Wenchao Sui[4], Meiling Sun[1,*]

[1]Department of Oncology, Yantai Hospital of Traditional Chinese Medicine, 264001 Yantai, Shandong, China
[2]Department of Pulmonary Diseases, Yantai Hospital of Traditional Chinese Medicine, 264001 Yantai, Shandong, China
[3]Clinical Teaching Department, Yantai Nurses School of Shandong, 264001 Yantai, Shandong, China
[4]Department of Oncology, Yantai Penglai Hospital of Traditional Chinese Medicine, 264000 Yantai, Shandong, China
*Correspondence: sml19860609@163.com (Meiling Sun)
†These authors contributed equally.
Published: 2 June 2023

Background: Cancer stem cells (CSCs) are characterized by an ability for unlimited proliferation and efficiency of self-renewal. The targeting of lung CSCs (LCSCs)-related signaling pathways represent a promising therapeutic strategy for treatment of lung cancer. Ferroptosis a potential strategy for LCSCs treatment, and curcumin cloud induce ferroptosis. In this study, we aimed to observe the effects of curcumin on LCSCs via ferroptosis-related pathways.
Methods: In this study, A549 cluster of differentiation (CD)133$^+$ and A549 CD133$^-$ cells were isolated using magnetic bead-based separation. Colony formation and sphere formation assays, as well as cells injection in non-obese diabetes/severe combined immune deficiency (NOD/SCID) mice, were used to analyze the tumorigenic ability of cells differentially expressing CD133. A549 CD133$^+$ cells were treated with different doses of curcumin (0, 10, 20, 40, 80 μM). Cell viability, glutathione peroxidase 4 (GPX4) and ferroptosis suppressor protein 1 (FSP1) expressions were measured. The 50% inhibitory concentration (IC_{50}) of curcumin, two ferroptosis inducers, inhibitor of GPX4 (RSL3) and inhibitor of FSP1 (iFSP1), and a ferroptosis inhibitor, ferrostatin-1 (Fer-1), were used to investigate the mechanism underlying the effect of curcumin on ferroptosis in A549 CD133$^+$ cells.
Results: A549 CD133$^+$ cells had greater tumorigenic ability than A549 cells. Curcumin treatment suppressed the expressions of GPX4 (glutathione peroxidase 4) and FSP1 in A549 CD133$^+$ cells, thereby inducing ferroptosis. RSL3 and iFSP1 respectively suppressed the GSH (glutathione)-GPX4 and FSP1 (ferroptosis suppressor protein 1)-CoQ10 (coenzyme Q10)-nicotinamide adenine dinucleotide (NADH) pathways in A549 CD133$^+$ cells. However, the roles of curcumin were blocked by Fer-1 treatment.
Conclusions: In this study, curcumin induced ferroptosis through inhibiting the GSH-GPX4 and FSP1-CoQ10-NADH pathways in A549 CD133$^+$ cells, resulting in the inhibition of their self-renewal potential.

Keywords: lung cancer stem cells; curcumin; Fer-1; iFSP1; RSL3

Introduction

Lung cancer is one of the most common malignant tumors worldwide and is associated with a high mortality rate [1,2]. Small cell cancer (SCLC) and non-small cell lung cancer (NSCLC)account for approximately 20% and 80% of total number of cases of lung cancer [2]. Despite the significant advances in diagnostic and therapeutic approaches, the prognosis of patients with lung cancer remains poor, mainly due to late diagnosis, drug resistance, and drug-related toxicity [2,3]. Consequently, further study new intervention targets and non-toxic therapeutic drugs for the management of this malignancy.

Cancer stem cells (CSCs) are characterized by unlimited proliferative capacity and self-renewal efficiency [4]. Increasing evidences confirm that CSCs are key controlling influencer in multiple tumor types, including lung cancer [5,6], through their influence on drug resistance, tumor progression and metastasis. Different criteria have been used to identify lung cancer stem cells (LCSCs), such as cell surface markers like cluster of differentiation (CD)44, CD133, and aldehyde dehydrogenase (ALDH) [7–10]. Targeting of LCSCs-related signaling pathways represent a promising therapeutic strategy for the treatment of lung cancer.

Ferroptosis is an iron-dependent and non-apoptotic cell death process, driven by aberrant metabolism and iron-dependent lipid peroxidation [11,12]. Several pathways have been found in the ferroptosis, including the GSH-GPX4 pathway, involving the depletion of glutathione (GSH) with glutathione peroxidase 4 (GPX4) suppression, and the FSP1-CoQ10-nicotinamide adenine dinucleotide (NADH) pathway, which entails the suppression of ferroptosis suppressor protein 1 (FSP1), with concurrent exhaus-

tion of NADH-dependent coenzyme Q10 (CoQ10) [13]. Moreover, FSP1 functions independently of cellular GSH-GPX4 pathway. Accumulating evidences have showed that ferroptosis can prevent cancer development through several oncogenic signaling pathways [12]. Inducing ferroptosis in cancer cells is thought to represent a promising strategy for the treatment of therapy-resistant cancers. Furthermore, SRY (sex determining region Y)-box transcription factor 2 (SOX2), a transcriptional factor with a key role in stem cell maintenance, was reported to confer resistance to ferroptosis via the activation of the cystine transporter solute carrier family 7 members 11 (SLC7A11) [14]. These observations suggest that inducing ferroptosis may be a feasible option for the LCSCs treatment.

Curcumin is a naturally occurring polyphenol derived from turmeric (*Curcuma longa*), that has a variety of biological activities against lung cancer [2,7]. A recent study showed that curcumin can induce ferroptosis through activating autophagy in NSCLC [1]. Understanding the potential mechanism of curcumin on ferroptosis is crucial to treatment NSCLC. Moreover, it has been reported that curcumin induces DNA damage in LCSCs [7], and also suppresses their self-renewal potential by suppressing Wingless-Int1 (Wnt)/β-catenin and Sonic Hedgehog pathways [9]. However, whether curcumin can also target LCSCs by inducing ferroptosis remains unclear.

In this study, we provided evidences that curcumin exerts ferroptosis-related effects against highly tumorigenic A549 cluster of differentiation (CD)133$^+$ cells by GSH-GPX4 and FSP1-CoQ10-NADH pathways.

Materials and Methods

Cell Culture

Human A549 NSCLC cells were purchased from Procell (#CL-0016, Procell Life Science & Technology Co., Ltd., Wuhan, China) and cultured in Dulbecco's modified Eagle's medium (DMEM) (#PM150210A, Procell, Wuhan, China) supplemented with 10% fetal bovine serum (FBS) and 1% penicillin/streptomycin (P/S) at 37 °C with 5% CO_2. The cells were tested for mycoplasma contamination and authenticated using short tandem repeats (STR) analysis (**Supplementary Materials**). The cells were seeded in well-plates at 70%–80% confluency. Details of the methodology used for cell maintenance and culture are provided in the **Supplementary Materials**.

A549 CD133$^+$ Cell Isolation

Based on previous reports [15,16], A549 CD133$^+$ cells were isolated by magnetic bead-based separation using Manual Ability Classification system (MACS, Miltenyi Biotech, Auburn, CA, USA). A549 cells were incubated with MicroBeads-labeled monoclonal anti-CD133 antibody (#130-097-049, Miltenyi Biotech, Auburn, CA, USA) at 4 °C for 30 min. The purity of the CD133$^+$ and CD133$^-$ cell populations was evaluated using a phycoerythrin (PE)-labeled antibody against human CD133 (#130-090-853, Miltenyi Biotech, Auburn, CA, USA) by flow cytometry.

Flow Cytometry

For CD133 staining, cells (1×10^6) were washed with phosphate buffer saline (PBS, #C0221A, Beyotime, Shanghai, China), treated with 1% bovine serum albumin (BSA, #ST023, Beyotime, Shanghai, China), then incubated with 2 μg/mL PE-conjugated mouse anti-human CD133 antibody (#130-090-853, Miltenyi Biotech, Auburn, CA, USA) at 4 °C for 30 min. The washed cells were harvested, filtrated, centrifuged, and subjected to flow cytometry (BD, FACSCanto II, Franklin Lakes, BJ, USA).

Immunofluorescence

Cells were fixed in 4% paraformaldehyde (#P0099, Beyotime, Shanghai, China) for 15 min, blocked with QuickBlock™ blocking buffer (#P0260, Beyotime, Shanghai, China) for 30 min, incubated with CD133 rabbit antibody (1:500, #51917, Cell Signaling Technology, China) overnight at 4 °C, and incubated with Alexa Fluor®594-conjugated goat anti-rabbit IgG (immunoglobulin G) (H+L) antibody (1:500, #8889, Cell Signaling Technology, Boston, MA, USA) at 37 °C for 60 min, then counterstained with 4',6-diamidino-2-phenylindole (DAPI) (#4083, Cell Signaling Technology, Boston, MA, USA). A confocal microscope (#LSM800, ZESS, Oberkochen, Germany) was used to observe and image the results.

Colony Formation Assay

As previously described [4,5], A549 CD133$^-$, A549 and A549 CD133$^+$ cells were resuspended in fresh DMEM with 10% FBS and 1% P/S, respectively. Approximately 80 cells per well were seeded into a six-well plate and cultured in RPMI (Roswell Park Memorial Institute)-1640 with 10% FBS for 10 days. Colony formation was assessed using crystal violet staining.

Sphere Formation Assay

Based on previous descriptions [4,5], A549 CD133$^-$, A549 and A549 CD133$^+$ cells were respectively cultured in DMEM containing 20 ng/mL epidermal growth factor (EGF) and 10 ng/mL basic fibroblast growth factor (bFGF) for 7 days. Sphere formation was observed under a microscope (#CKX53, Olympus, Nagoano, Japan).

Animals

Forty male non-obese diabetes/severe combined immune deficiency (NOD/SCID) mice (Beijing Vital River Company, Beijing, China), aged 6–8 weeks and weighting 18–25 g, were housed per cage in a sterile environment under a 12-h/12-h light-dark cycle and with free access to food and water. After 7 days, mice were used to study.

In Vivo Tumorigenicity Assay

Following anesthesia with 1% pentobarbital sodium (45 mg/kg), A549 CD133$^-$, A549 or A549 CD133$^+$ cells (3×10^6) were subcutaneously injected into the right flanks of NOD/SCID mice (5 mice per group). Tumor volumes (length $\times$ width^2 $\times$ 0.5) were measured every 7 days after implantation. After 28 days of injection, the anesthetized mice (1% pentobarbital sodium) were euthanized to obtain tumor tissues.

Inhibition of Curcumin on A549 CD133$^+$ Cells

Curcumin (#805204, Macklin, Shanghai, China) was dissolved in 0.1% dimethyl sulfoxide (DMSO). A549 CD133$^+$ cells were cultured for 48 h with different concentrations (10, 20, 40 and 80 μmol/L) of curcumin. Cells treated with 0.1% DMSO served as controls.

A549 CD133$^+$ cells (1×10^4 per well) were cultured for 48 h at 37 °C with 5% CO_2. Then, 10 μL of cell counting kit-8 (CCK-8) solution (#C0037, Beyotime, Shanghai, China) was added to each well for 4 h. Absorbance at 450 nm was read using a microplate reader (#ELx808, BioTek, Winooski, VT, USA). The 50% inhibitory concentration (IC_{50}) of curcumin was analyzed to following experiments.

A549 CD133$^+$ Cells Treatments

A549 CD133$^+$ cells were divided into the following groups: Control group, curcumin group, RSL3 (inhibitor of GPX4) group, iFSP1 (inhibitor of FSP1) group, and curcumin plus Fer-1 (ferrostatin-1) group.

In the control group, cells were cultured with 0.1% DMSO for 48 h.

In the curcumin group, cells were cultured with curcumin at the IC_{50} for 48 h.

In the RSL3 group, cells were cultured with 10 μmol/L RSL3 (#S8155, Selleck, Shanghai, China) [17] for 48 h.

In the iFSP1 group, cells were cultured with 10 μmol/L iFSP1 (#S9663, Selleck, Shanghai, China) [18] for 48 h.

In the curcumin plus Fer-1 group, cells were cultured with curcumin at the IC_{50} and 10 μmol/L ferrostatin-1 (Fer-1) (#S7243, Selleck, Shanghai, China) [1] for 48 h.

Determination of Reactive Oxygen Species (ROS) Levels in A549 CD133$^+$ Cells

A fluorometric intracellular ROS kit (#MAK144, Sigma, Shanghai, China) was used to analyze cellular ROS levels. 100 μL of kit solution was added to cells (1×10^4 per well) for 20 min shield from light. After washing, the fluorescence was determined by flow cytometry (BD, FACSCanto II, Franklin Lakes, BJ, USA).

Detection of GSH and NADH Level in A549 CD133$^+$ Cells

The GSH levels in each group were analyzed using a GSH/glutathione disulfide (GSSG) assay kit (#S0053, Beyotime, Shanghai, China). Total GSH (GSH + GSSG) levels were measured through analyzing absorbance at 420 nm using glutathione reductase to reduce GSSG to GSH. GSSG was calculated by removing endogenous GSH with a GSH scavenger.

The cellular NAD$^+$/NADH in each group were analyzed using a NAD$^+$/NADH assay kit (#S0175, Beyotime, Shanghai, China). Following the manufacturer's instructions, the washed (cold PBS) cells were harvested and homogenized in NAD$^+$/NADH extraction buffer. The absorbance of NAD$^+$ and NADH was observed at 340 nm using a microplate reader (#ELx808, BioTek, Winooski, VT, USA).

Detection of CoQ10 Levels in A549 CD133$^+$ Cells

The harvested cells of each group were incubated with protein lysis buffer, homogenized and stored at –20 °C. After two freeze-thaw cycles, the intracellular CoQ10 levels in supernatant of cells were detected using a CoQ10 ELISA kit (#abx159767, Abbexa, Cambridge, UK).

Western Blotting

Western blotting was performed as previously reported [19]. After extraction, equal amounts of cellular protein (30 μg) were separated by 12% sodium dodecyl sulfate-polyacrylamide gel electrophoresis (Mini Protean 3 Dodeca, SDS-PAGE, BD, Franklin Lakes, BJ, USA), and transferred to polyvinylidene fluoride membranes. The blocked membranes were incubated with rabbit antibodies, targeting GPX4 (1:1000, #DF6701, Affinity, Liyang, China), FSP1 (1:1000, #A19109, ABclonal, Wuhan, China), and GAPDH (1:1000, #AC001, ABclonal, Wuhan, China) overnight at 4 °C, and incubated with HRP (horseradish peroxidase)-conjugated anti-rabbit IgG (H+L) antibody (1:1000, #AS029, ABclonal, Wuhan, China) for 60 min at 37 °C. An enhanced chemiluminescence substrate detection kit (#K1230, Apexbio, Shanghai, China) was implemented to visualize the protein bands.

Animal Treatments

A549 CD133$^+$ cells (3×10^5) were subcutaneously injected into the right flanks of anesthetized NOD/SCID mice. After 4 days of injection, 25 male mice were randomly divided into the following groups (5 mice per group): Control group, curcumin group, RSL3 group, iFSP1 group, and curcumin plus Fer-1 group.

In the control group, mice received 0.1% DMSO intraperitoneally every day for 24 days.

In the curcumin group, mice were intraperitoneally treated with 100 mg/(kg·d^{-1}) curcumin [1] for 24 days.

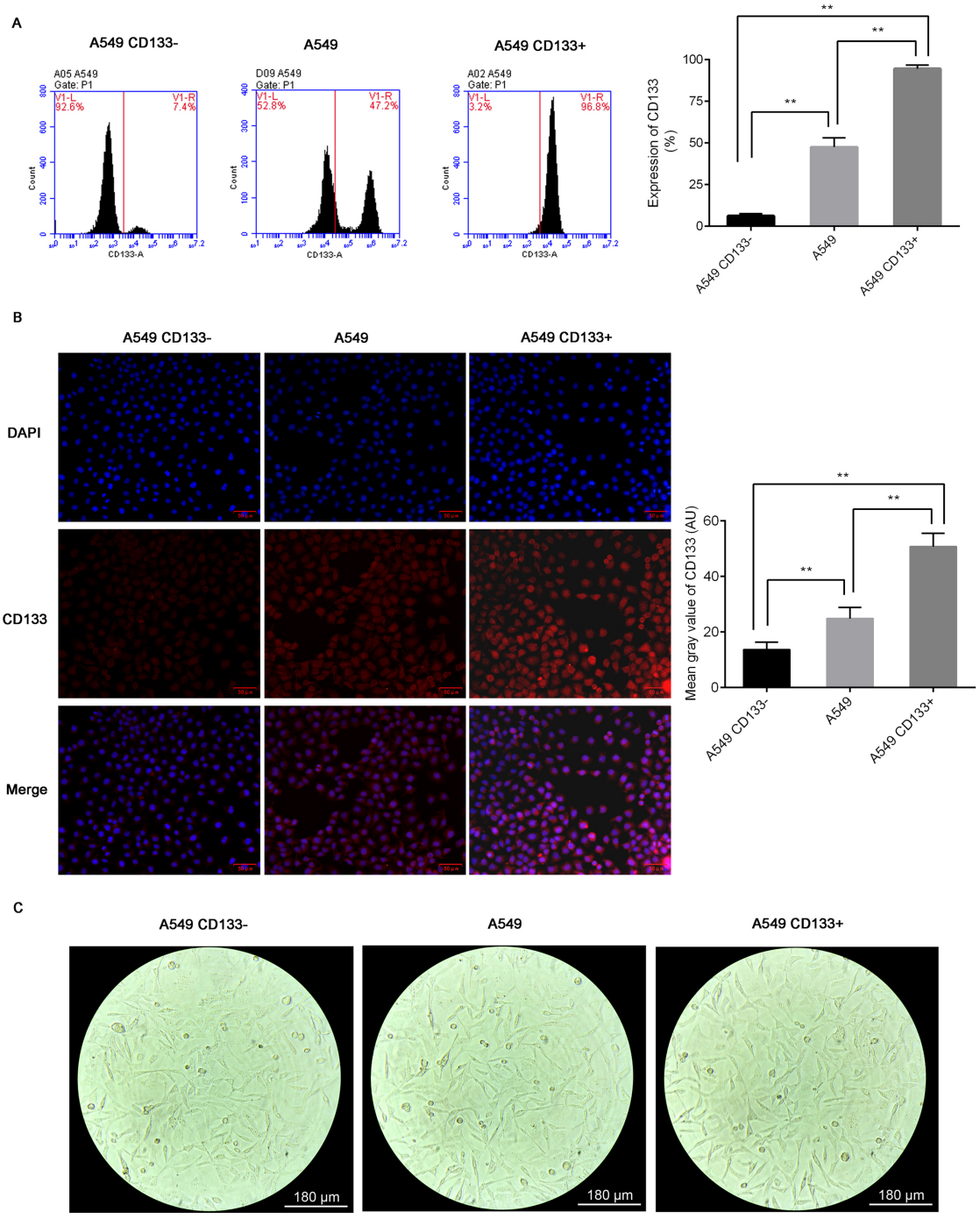

Fig. 1. Isolation of A549 CD133$^-$ cells and A549 CD133$^+$ subpopulations from A549 cells. The CD133 expression in cells was analyzed by flow cytometry (A) and immunofluorescence staining (B). Three replicates were performed (scale = 50 μm). (C) Cells morphology. $^{**}p < 0.01$.

In the RSL3 group, mice were administrated with 100 mg/(kg·d^{-1}) RSL3intraperitoneally [17] for 24 days.

In the iFSP1 group, mice were received with 100 mg/(kg·d^{-1}) iFSP1 intraperitoneally for 24 days.

In the curcumin plus Fer-1 group, the mice were intraperitoneally treated with 100 mg/(kg·d^{-1}) curcumin and mg/(kg·d^{-1}) Fer-1 for 24 days.

Determination of Tumor Size and Weight

Tumor size (width^2 $\times$ depth $\times$ 0.5) was estimated every week. After 28 days, all mice were anesthetized (1% pentobarbital sodium) and euthanized by decapitation. Tumor tissues was then removed, and the tumor weights were obtained.

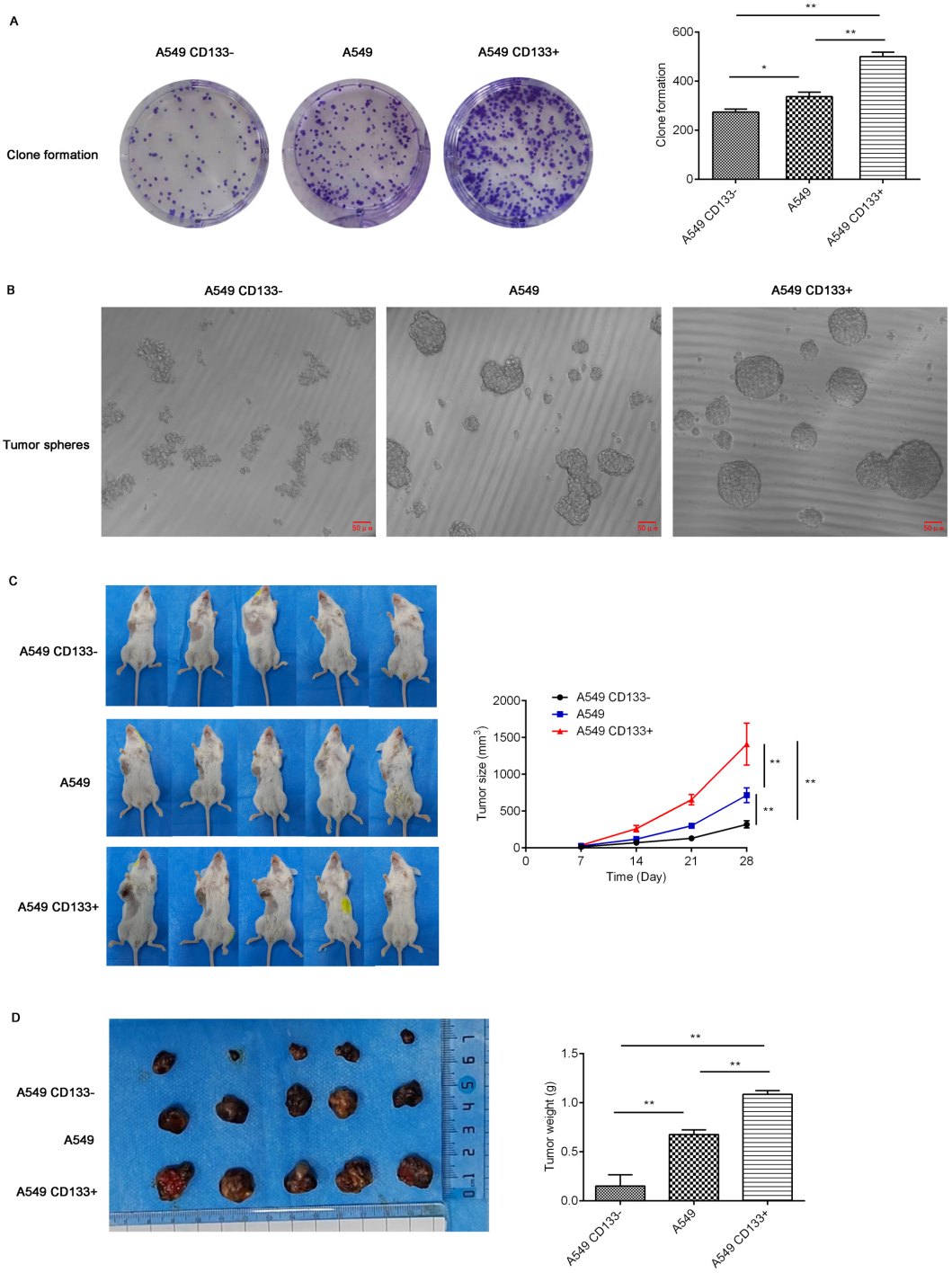

Fig. 2. Comparison of the tumorigenic capacity of cells with differential CD133 expression. (A) Clone formation assay (n = 3) were performed in 6 well cell culture plates (127 × 85.5 × 23 mm). (B) Sphere formation assay (n = 3) (scale = 50 μm). (C) NOD/SCID mice tumorigenicity assay, and tumor size was measured every week (n = 5). (D) Tumor weight was analyzed (n = 5). $^{*}p < 0.05$, $^{**}p < 0.01$.

Hematoxylin and Eosin (H&E)

Tumor fixed tissues (4% paraformaldehyde, 24 h) were dehydrated with ethanol (80%, 90%, 95%, and 100%, 2 h each), embedded in paraffin, dewaxed with xylene (10 min, then 5 min), rehydrated with ethanol (100%, 100%, 95%, 90%, and 85%, 1 min each), sectioned (3-μm-thick slices), and stained with H&E solution (#G1120, Solarbio, Beijing, China) for 4 min. After dehydrating using a graded ethanol series (85%, 20 s; 90%, 30 s; 95%, 1 min, twice; 100%, 2 min, twice), the tissues were cleared with xylene, sealed, and visualized.

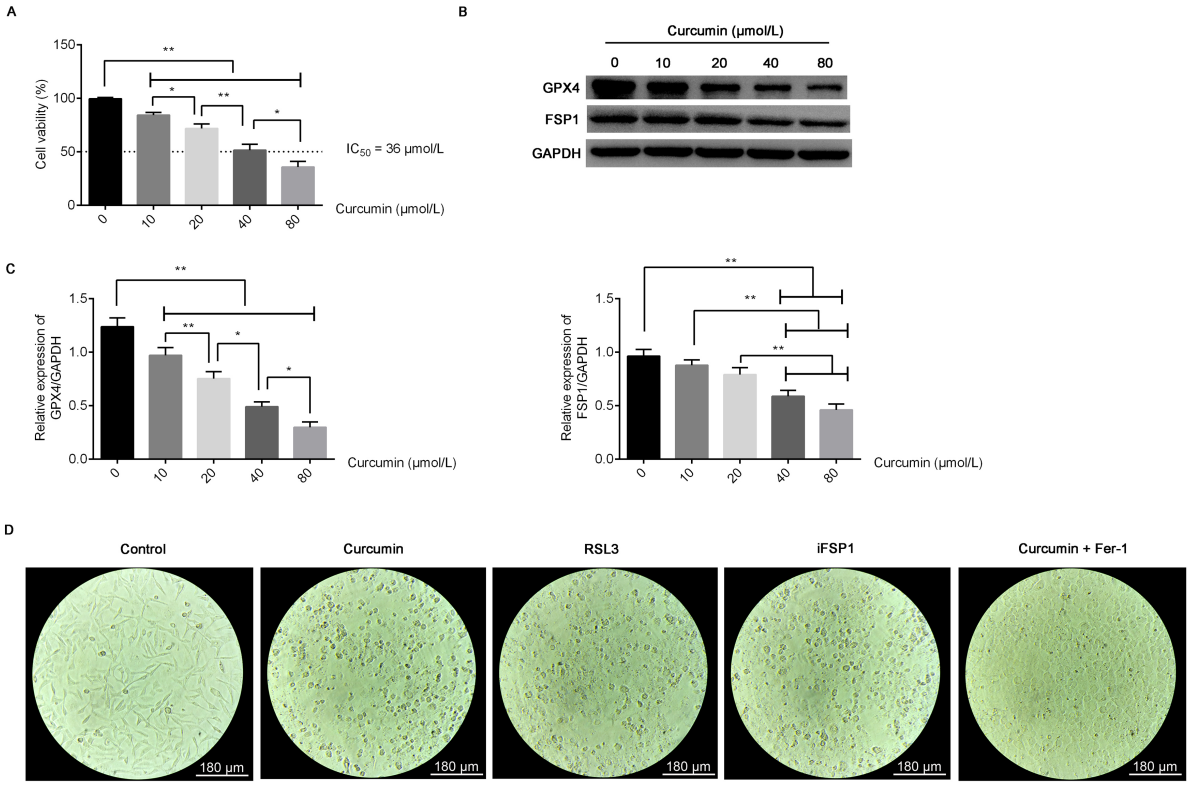

Fig. 3. The ferroptosis-inducing efficacy of curcumin in A549 CD133$^+$ cells. (A) Cell viability was detected by a CCK-8 kit (n = 3). (B) Expressions of GPX4 and iFSP1 proteins were analyzed by western blotting (n = 3). (C) Relative expression of GPX4 and iFSP1 proteins was quantified by Image J software (V1.8.0.112, National Institutes of Health, Bethesda, MD, USA) (n = 3). (D) Cell morphology was observed under a light microscope. $^*p < 0.05$, $^{**}p < 0.01$.

Immunohistochemistry

Hydrated slices (3-μm-thick) were cultured in 3% H_2O_2 for 30 min at 37 °C and boiled in sodium citrate buffer for 10 min, twice. The washed slices were incubated with rabbit antibodies Ki-67 (1:300, #AF0198, Affinity, Liyang, China), GPX4 (1:300, #DF6701, Affinity, Liyang, China), and FSP1 (1:300, #A19109, ABclonal, Wuhan, China) overnight at 4 °C, then incubated with the secondary antibody (1:5000, #S0001, Affinity, Liyang, China) for 30 min at 37 °C, and stained with diaminobenzidine. Finally, the slices were dehydrated, cleared, and sealed.

Statistics

Data were analyzed by SPSS20.0 (National Institutes of Health, Bethesda, MD, USA) and shown as mean ± standard deviation by GraphPad Prism 8.0 (GraphPad Software Inc., San Diego, CA, USA) and One-way analysis of variance followed Tukey's test was implemented to compare differences among multiple groups. A p-value < 0.05 was considered significant.

Results

Isolation of A549 CD133$^-$ and A549 CD133$^+$ Cells

The separated A549 cells were analyzed by flow cytometry (Fig. 1A) and immunofluorescence staining (Fig. 1B) for CD133 expression. CD133 expression was detected in 47.2% of A549 cells, 7.4% of A549 CD133$^-$ cells, and 96.8% of A549 CD133$^+$ cells ($p < 0.01$). The results indicated a good enrichment of CD133 subpopulations. Meanwhile, the cell morphology of A549 CD133$^-$, A549 and A549 CD133$^+$ cells was observed to be polygonal, and no difference in morphology was detected among the three A549 subpopulations (Fig. 1C).

Comparison of the Tumorigenic Ability of Cells with Different CD133 Expression

The tumorigenicity potential of cells with differential CD133 expression was observed using colony formation (Fig. 2A), sphere formation (Fig. 2B), and NOD/SCID mice tumorigenicity assays (Fig. 2C,D). The results showed that A549 CD133$^+$ cells possessed greater tumorigenic capacity than A549 cells ($p < 0.01$), while A549 CD133$^-$ cells showed lower tumorigenic ability than A549 cells ($p < 0.05$).

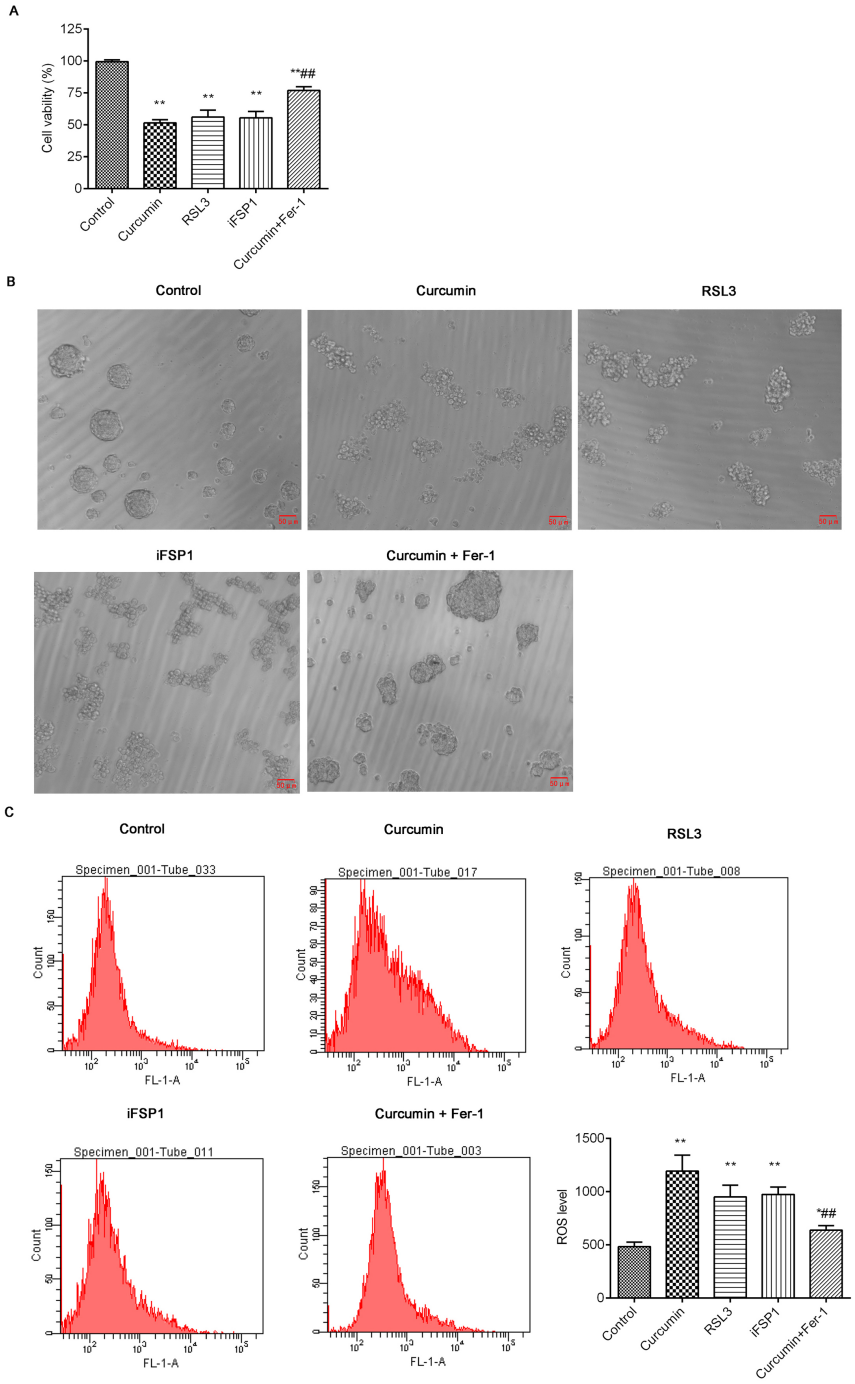

Fig. 4. Effects of curcumin on ferroptosis in A549 CD133$^+$ cells. Cells were respectively cultured with 36 μM curcumin, 10 μmol/L RSL3, 10 μmol/L iFSP1, or 10 μmol/L Fer-1 for 48 h. (A) After 48 h of treatment, cell viability was detected by a CCK-8 kit (n = 3). (B) Sphere forming ability was analyzed by a sphere formation assay (n = 3) (scale = 50 μm). (C) Cellular ROS levels were analyzed by a fluorometric intracellular ROS kit (n = 3). $^*p < 0.05$, $^{**}p < 0.01$ vs. the control group. $^{\#\#}p < 0.01$ vs. the curcumin group.

Effects of Curcumin on Ferroptosis in A549 CD133$^+$ Cells

Next, to check the ferroptosis-inducing efficacy of curcumin in A549 CD133$^+$ cells, we used different doses of curcumin (10, 20, 40, 80 μM) to treat cells. The cell viability was clearly decreased in a curcumin dose-dependent manner (Fig. 3A) ($p < 0.05$). Importantly, the expressions of GPX4 and FSP1 protein were clearly downregulated, and this effect was also dependent on the dose of curcumin administered (Fig. 3B,C) ($p < 0.05$). The IC_{50} (36 μM) of curcumin was analyzed and used in the following experiments.

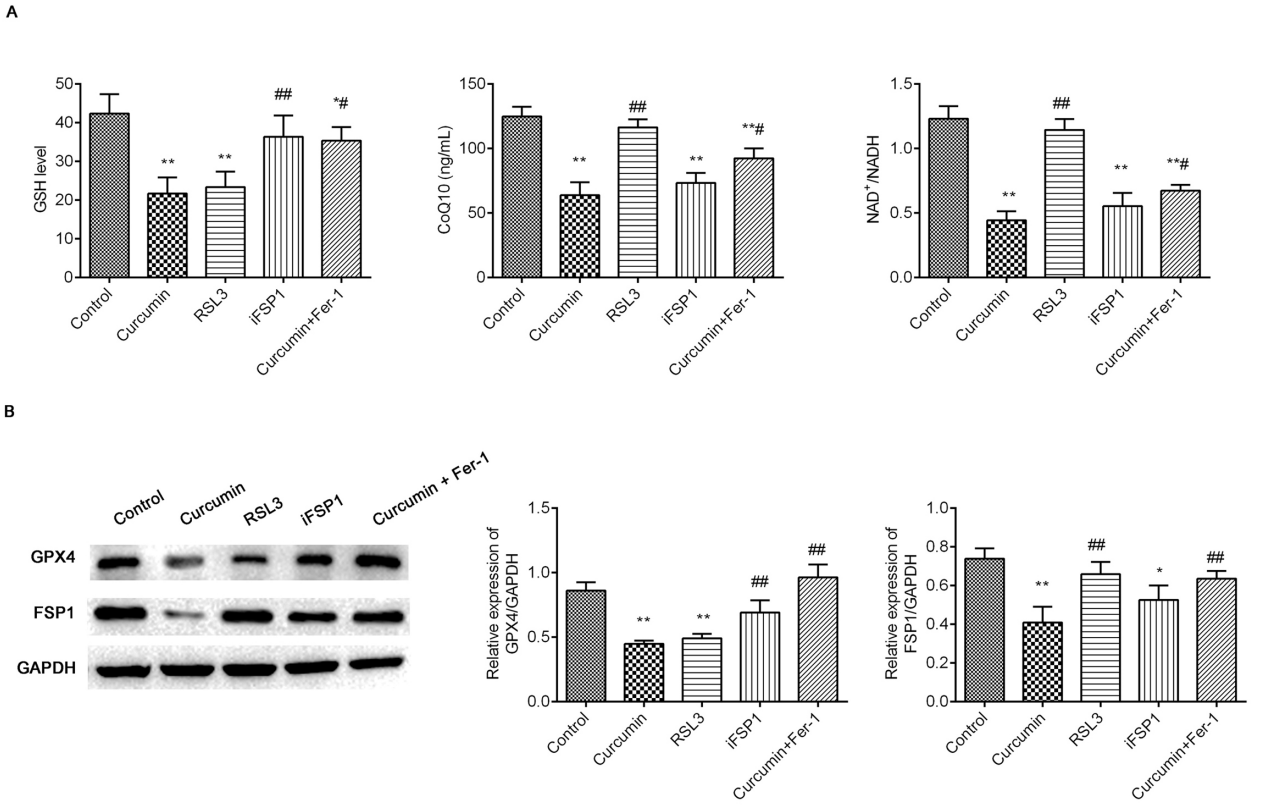

Fig. 5. Curcumin induced ferroptosis in A549 CD133$^+$ cells through the GSH-GPX4 and FSP1-CoQ10-NAPH pathways. (A) The GSH level, NAD$^+$/NADH and CoQ10 level were detected in cells (n = 3). (B) The expressions of GPX4 and FSP1 proteins were analyzed in cells (n = 3). $^*p < 0.05$, $^{**}p < 0.01$ vs. the control group. $^{\#}p < 0.05$, $^{\#\#}p < 0.01$ vs. the curcumin group.

To confirm that curcumin induces ferroptosis in A549 CD133$^+$ cells through the GSH-GPX4 and FSP1-CoQ10-NAPH pathways, cells were divided into five treatment groups and their respective morphologies of each group was observed (Fig. 3D). We found that the polygon shape disappeared in cell treated with curcumin. The same effect was observed with RSL3 (an inducer of ferroptosis, inhibitor of GPX4) or iFSP1 (an inducer of ferroptosis, inhibitor of iFSP1) treatment. However, Fer-1 (a selective inhibitor of ferroptosis) treatment blocked the effect of curcumin on cell morphology.

Curcumin Induced Ferroptosis in A549 CD133$^+$ Cells through the GSH-GPX4 and FSP1-CoQ10-NAPH Pathways

The A549 CD133$^+$ cells viability of each group was analyzed (Fig. 4A). We found that the cell viability was clearly suppressed by treatment with curcumin, RSL3, or iFSP1 contrasted to that seen in the control cells ($p < 0.01$). However, the cell viability was obviously enhanced in cells treated with curcumin + Fer-1 relative to that in cells treated with curcumin alone ($p < 0.01$). In the sphere formation assay (Fig. 4B), meanwhile, the sphere forming ability of A549 CD133$^+$ cells was clearly suppressed with curcumin, RSL3, or iFSP1 treatment compared with that seen in the control condition. However, Fer-1 weakened the inhibitory effects of curcumin on sphere formation in A549 CD133$^+$ cells. We also measured the ROS levels in A549 CD133$^+$ cells in each group (Fig. 4C), and found that ROS levels were higher in the curcumin, RSL3, or iFSP1 treatment groups than that in the control group ($p < 0.01$). Contrasted to the curcumin alone treatment, the ROS levels were greatly downregulated in the cells treated with curcumin + Fer-1 ($p < 0.01$).

Next, we measured the levels of GSH, CoQ10, and NAD$^+$/NADH in cells of each group (Fig. 5A). By contrast to the control condition, the above indicators were significantly decreased after curcumin treatment ($p < 0.01$), as was the expressions of GPX4 and FSP1 proteins ($p < 0.01$) (Fig. 5B). Importantly, the Fer-1 administration obviously suppressed these curcumin-mediated effects ($p < 0.01$). Furthermore, the RSL3 treatment significantly suppressed the GSH level and GPX4 expression ($p < 0.01$), but did not affect the CoQ10 level, NAD$^+$/NADH, or FSP1 expression ($p > 0.05$). Meanwhile, the iFSP1 treatment significantly suppressed the CoQ10 level, NAD$^+$/NADH, and FSP1 expression ($p < 0.01$), but did not affect the GSH level, or GPX4 expression ($p > 0.05$).

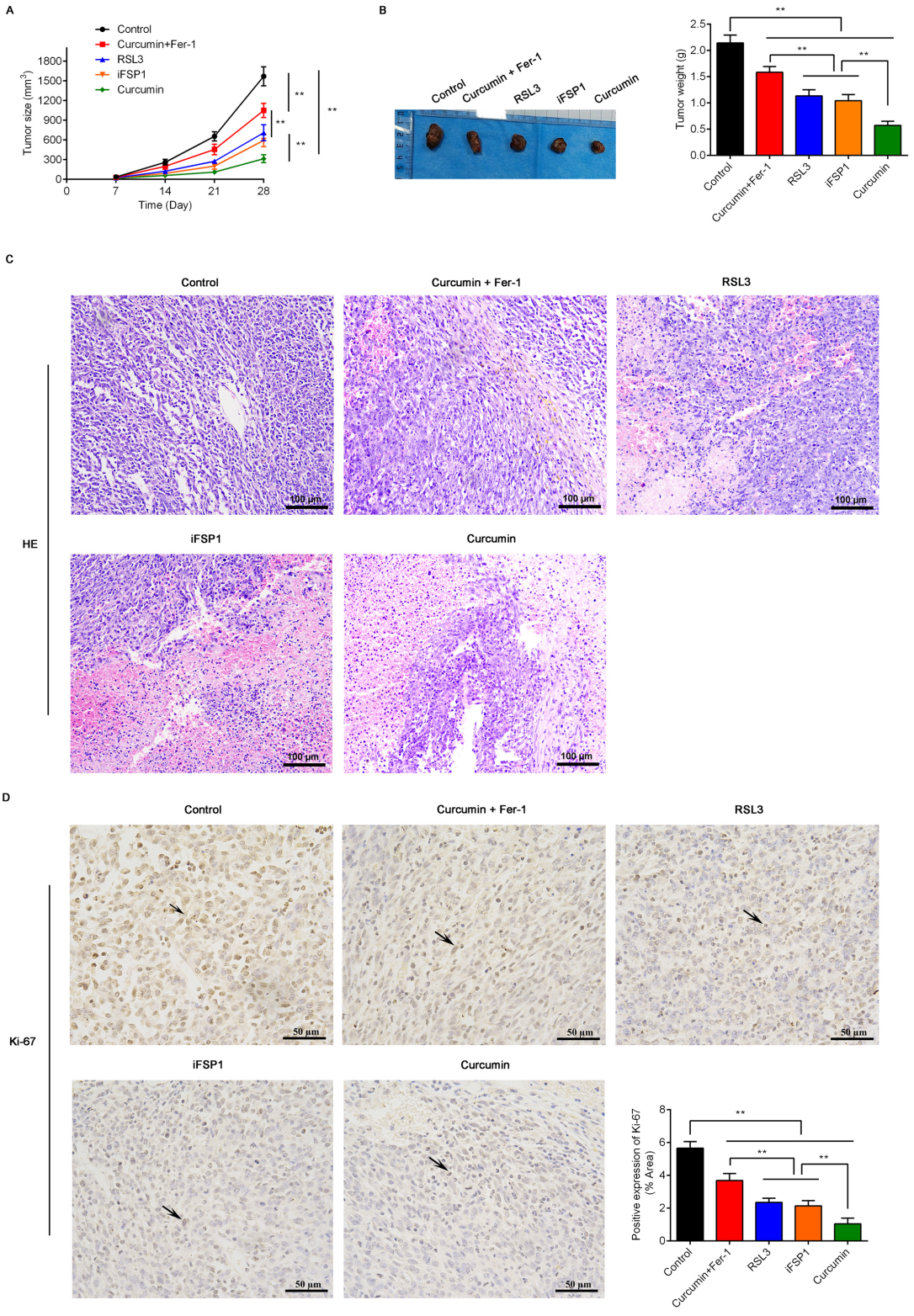

Fig. 6. Curcumin induced ferroptosis in NOD/SCID mice injected with A549 CD133$^+$ cells. Four days after A549 CD133$^+$ cells injection, 25 male NOD/SCID mice were respectively intraperitoneally treated with curcumin (100 mg/kg·d), RSL3 (100 mg/kg·d), iFSP1 (100 mg/kg·d), or Fer-1 (100 mg/kg·d) for 24 days (n = 5). (A) Tumor size in each group. (B) Tumor weight in each group. (C) Tumor pathology in each group (scale = 100 μm). (D) Ki-67 expression in each group (scale = 50 μm). Black arrows indicate Ki-67 expression. $^{**}p < 0.01$.

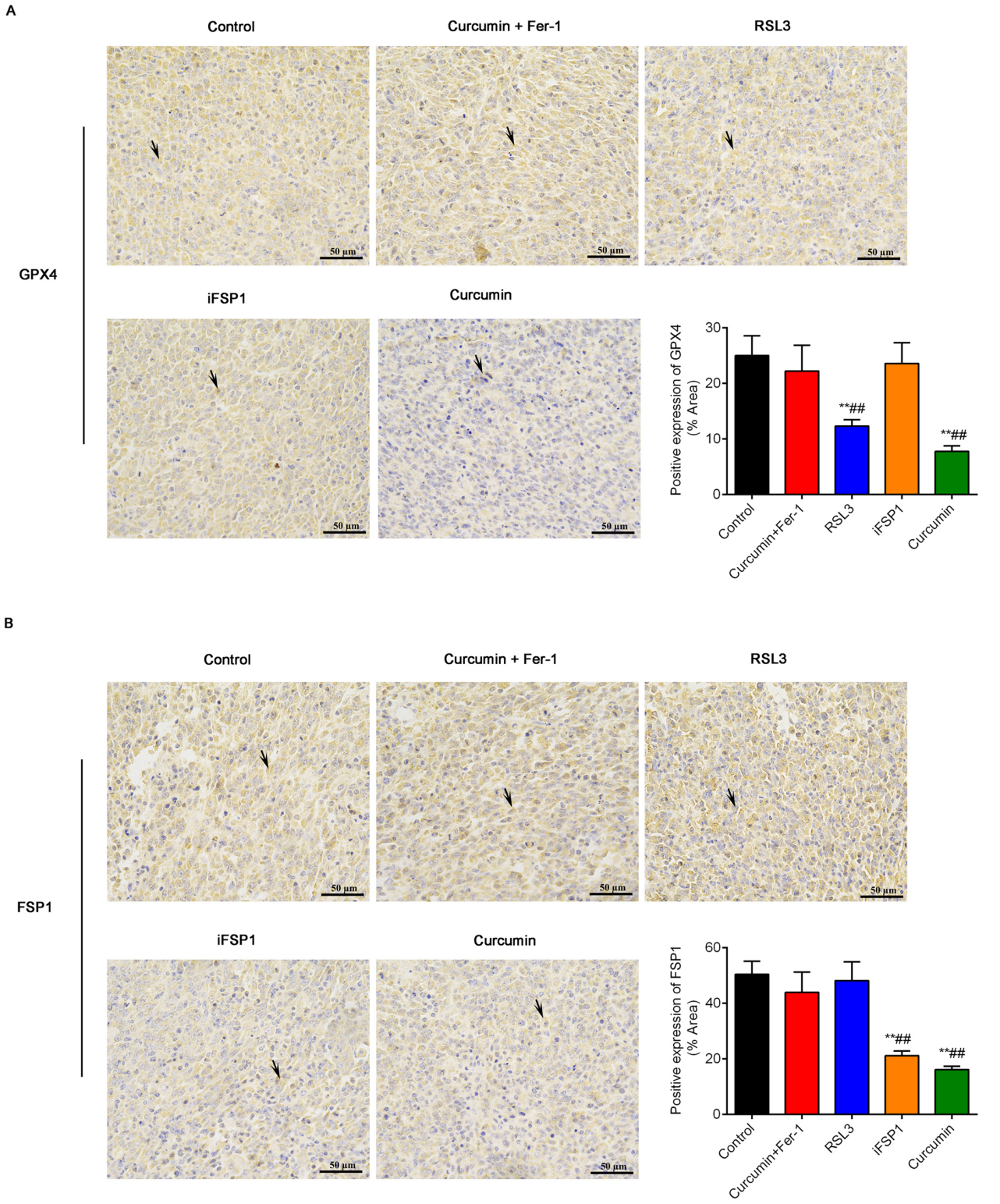

Fig. 7. Effects of curcumin on GPX4 and FSP1 protein expression in tumor tissues of NOD/SCID mice injected with A549 CD133^{+} cells. The expressions of GPX4 (A) and FSP1 (B) in tumor tissues of each group were analyzed by immunohistochemistry (n = 5) (scale = 50 μm). $^{**}p < 0.01$ vs. the control group. $^{\#\#}p < 0.01$ vs. the curcumin + Fer-1 group.

Curcumin Induced Ferroptosis through the GSH-GPX4 and FSP1-CoQ10-NAPH Pathways in NOD/SCID Mice Injected with A549 CD133$^+$ Cells

In vivo study, we injected A549 CD133$^+$ cells into NOD/SCID mice, and then compared the tumor size (Fig. 6A) and tumor weight (Fig. 6B) among the different treatment groups. The results showed that tumor growth was markedly suppressed in the curcumin, RSL3, or iFSP1 groups relative to that in the control group ($p < 0.01$). Curcumin, RSL3, or iFSP1 treatment also improved tumor pathology (Fig. 6C) as well as suppressed Ki-67 expressions in tumors (Fig. 6D). Furthermore, the tumor-inhibiting effects of curcumin were superior to those of RSL3 or iFSP1 ($p < 0.01$). However, the Fer-1 administration clearly suppressed the antitumor effects of curcumin ($p < 0.01$).

Effects of Curcumin on GPX4 and FSP1 Expression in NOD/SCID Mice Injected with A549 CD133$^+$ Cells

The expression of GPX4 (Fig. 7A) and FSP1 (Fig. 7B) in tumor tissues of each group was observed. The GPX4 and FSP1 positive expressions were significantly downregulated after curcumin treatment by contrast to the control group ($p < 0.01$). While, the Fer-1 treatment clearly suppressed the effects of curcumin on GPX4 and FSP1 expression. Additionally, the RSL3 treatment noticeably inhibited the GPX4 expression ($p < 0.01$), but did not affect the FSP1 expression contrasted to the control group. In contrast, the iFSP1 treatment clearly inhibited the FSP1 expression compared with that in the control group ($p < 0.01$), whereas the GPX4 expression was unaffected by the iFSP1 treatment.

Discussion

It has been demonstrated that CSCs are key drivers of tumor invasion, metastasis and relapse, and are also the primary cause of the chemo-resistant phenotype [8,20]. LCSCs are well-recognized using specific markers, such as CD133, CD44, and ALDH1 as well as their CSCs characteristics such as colony formation and spheroid formation abilities [8]. In our study, we successfully isolated A549 CD133$^+$ cells using magnetic bead-based separation and found that the fraction of CD133$^+$-expressing cells among A549 cells was greater than 90%. Furthermore, our data showed that A549 CD133$^+$ cells displayed higher tumorigenic potential than A549 cells as determined by colony formation, sphere formation, and tumorigenicity assays in NOD/SCID mice. These findings indicated that A549 CD133$^+$ cells possessed features of cancer-initiating stem-like cells, in line with previous reports [6,15].

It has been reported that curcumin can significantly decrease the self-renewal ability of LCSCs [7] via a mechanism that may involve the suppression of the Wnt/β-catenin and Sonic Hedgehog pathways [9]. Furthermore, curcumin can induce ferroptosis by activating autophagy, thereby inhibiting NSCLC [1]. However, whether curcumin can activate ferroptosis inn LCSCs has remained unclear. In this work, we found that curcumin treatment can suppress the expressions of GPX4 and FSP1 in A549 CD133$^+$ cells, suggesting that curcumin might induce ferroptosis in LCSCs through the GSH-GPX4 and FSP1-CoQ10-NADH pathways. GPX4, a GSH-dependent enzyme, plays a key role in ferroptosis through decreasing lipid peroxidation contents. Additionally, GSH reductase utilizes NADPH to reduce glutathione-S-S-glutathione (GSSG) to G-SH, thereby preventing lipid ROS accumulation [21,22]. Independently of the GSH-GPX4 pathway, FSP1, an NADH-dependent CoQ oxidoreductase, prevents lipid peroxidation and also induces ferroptosis [22]. Blocking GPX4 or FSP1 can significantly increase sensitivity to ferroptosis, resulting in the suppression of many cancers [22,23].

In order to confirm our hypothesis, we used two ferroptosis inducers (RSL3 and iFSP1) and a ferroptosis inhibitor (Fer-1) to analyze the mechanism of curcumin on ferroptosis in A549 CD133$^+$ cells. As a ferroptosis inducer, RSL3 induces ferroptosis through GPX4 inhibition [24]. Meanwhile, iFSP1 induces ferroptosis through FSP1 inhibition [18]. As a ferroptosis inhibitor, Fer-1 inhibits ferroptosis by scavenging the initial alkoxyl radicals and other rearrangement products produced by ferrous oxide from lipid hydroperoxides; However, the Fer-1itself is not consumed in this process [25]. In our study, we found that RSL3 and iFSP1 respectively suppressed the GSH-GPX4 and FSP1-CoQ10-NADH pathways in A549 CD133$^+$ cells. Our results also showed that curcumin induced ferroptosis by inhibiting GPX4 and FSP1 in A549 CD133$^+$ cells. However, the roles of curcumin were hampered by Fer-1 treatment.

However, the ability of curcumin to target LCSCs may be due to its unique potential to specifically target intermediate molecules in LCSCs mediated signaling pathways. Further in-depth investigation is required to confirm the role of curcumin in ferroptosis in LCSCs.

Conclusions

In summary, this work depicted the curcumin induced ferroptosis by inhibiting the GSH-GPX4 and FSP1-CoQ10-NADH pathways in A549 CD133$^+$ cells, resulting in the inhibition of self-renewal potential. These data contribute to explaining the mechanism underlying the preventive effect of curcumin against LCSCs mediated tumorigenesis.

Availability of Data and Materials

All data generated in this published article and supplementary information files for further data are available from the corresponding author.

Author Contributions

JZ, LZ and MS—designed the research study; JZ, LZ and AH—performed the research; WS and MS—provided help and advice on the animal experiment; JY and WS—analyzed the data. All authors contributed to editorial changes in the manuscript. All authors read and approved the final manuscript. All authors have participated sufficiently in the work and agreed to be accountable for all aspects of the work.

Ethics Approval and Consent to Participate

The protocols of animal experiments were in compliance with the revised Animals (Scientific Procedures) Act 1986 in the UK and Directive 2010/63/EU in Europe, and were reviewed and approved by the Ethics Committee of Yantai Hospital of Traditional Chinese Medicine (Approval number 2021-75-KY).

Acknowledgment

This manuscript was edited by the Charlesworth Author Services.

Funding

This work was supported by the Natural Science Foundation of Shandong Province (No. ZR2021QH023).

Conflict of Interest

The authors declare no conflict of interest.

Supplementary Material

Supplementary material associated with this article can be found, in the online version, at https://doi.org/10.24976/Discov.Med.202335176.26.

References

[1] Tang X, Ding H, Liang M, *et al*. Curcumin induces ferroptosis in non-small-cell lung cancer via activating autophagy. *Thorac Cancer.* 2021;12(8):1219–1230. doi: 10.1111/1759-7714.13904

[2] Wan Mohd Tajuddin WNB, Lajis NH, Abas F, Othman I, Naidu R. Mechanistic Understanding of Curcumin's Therapeutic Effects in Lung Cancer. *Nutrients.* 2019;11(12):2989. doi: 10.3390/nu11122989

[3] Imran M, Ullah A, Saeed F, Nadeem M, Arshad MU, Suleria HAR. Cucurmin, anticancer, & antitumor perspectives: A comprehensive review. *Crit Rev Food Sci Nutr.* 2018;58(8):1271–1293. doi: 10.1080/10408398.2016.1252711

[4] Meng X, Li M, Wang X, Wang Y, Ma D. Both CD133+ and CD133- subpopulations of A549 and H446 cells contain cancer-initiating cells. *Cancer Sci.* 2009;100(6):1040–1046. doi: 10.1111/j.1349-7006.2009.01144.x

[5] Hao S, Zhu X, Liu Z, *et al*. Chronic intermittent hypoxia promoted lung cancer stem cell-like properties via enhancing Bach1 expression. *Respir Res.* 2021;22(1):58. doi: 10.1186/s12931-021-01655-6

[6] Moro M, Bertolini G, Pastorino U, Roz L, Sozzi G. Combination Treatment with All-Trans Retinoic Acid Prevents Cisplatin-Induced Enrichment of CD133+ Tumor-Initiating Cells and Reveals Heterogeneity of Cancer Stem Cell Compartment in Lung Cancer. *J Thorac Oncol.* 2015;10(7):1027–1036. doi: 10.1097/JTO.0000000000000563

[7] Mirza S, Vasaiya A, Vora H, Jain N, Rawal R. Curcumin Targets Circulating Cancer Stem Cells by Inhibiting Self-Renewal Efficacy in Non-Small Cell Lung Carcinoma. *Anticancer Agents Med Chem.* 2017;17(6):859–864. doi: 10.2174/1871520616666160923102549

[8] Prabavathy D, Swarnalatha Y, Ramadoss N. Lung cancer stem cells-origin, characteristics and therapy. *Stem Cell Investig.* 2018;5:6. doi: 10.21037/sci.2018.02.01

[9] Zhu JY, Yang X, Chen Y, *et al*. Curcumin Suppresses Lung Cancer Stem Cells via Inhibiting Wnt/β-catenin and Sonic Hedgehog Pathways. *Phytother Res.* 2017;31(4):680–688. doi: 10.1002/ptr.5791

[10] Zeuner A, Francescangeli F, Contavalli P, *et al*. Elimination of quiescent/slow-proliferating cancer stem cells by Bcl-XL inhibition in non-small cell lung cancer. *Cell Death Differ.* 2014;21(12):1877–1888. doi: 10.1038/cdd.2014.105

[11] Jiang X, Stockwell BR, Conrad M. Ferroptosis: mechanisms, biology and role in disease. *Nat Rev Mol Cell Biol.* 2021;22(4):266–282. doi: 10.1038/s41580-020-00324-8

[12] Wu M, Zhang X, Zhang W, *et al*. Cancer stem cell regulated phenotypic plasticity protects metastasized cancer cells from ferroptosis. *Nat Commun.* 2022;13(1):1371. doi: 10.1038/s41467-022-29018-9

[13] Yang M, Tsui MG, Tsang JKW, *et al*. Involvement of FSP1-CoQ_10-NADH and GSH-GPx-4 pathways in retinal pigment epithelium ferroptosis. *Cell Death Dis.* 2022;13(5):468. doi: 10.1038/s41419-022-04924-4

[14] Wang X, Chen Y, Wang X, *et al*. Stem Cell Factor SOX2 Confers Ferroptosis Resistance in Lung Cancer via Upregulation of SLC7A11. *Cancer Res.* 2021;81(20):5217–5229. doi: 10.1158/0008-5472.CAN-21-0567

[15] Bertolini G, Roz L, Perego P, *et al*. Highly tumorigenic lung cancer CD133+ cells display stem-like features and are spared by cisplatin treatment. *Proc Natl Acad Sci U S A.* 2009;106(38):16281–16286. doi: 10.1073/pnas.0905653106

[16] Tirino V, Camerlingo R, Bifulco K, *et al*. TGF-β1 exposure induces epithelial to mesenchymal transition both in CSCs and non-CSCs of the A549 cell line, leading to an increase of migration ability in the CD133+ A549 cell fraction. *Cell Death Dis.* 2013;4(5):e620. doi: 10.1038/cddis.2013.144

[17] Zhang X, Sui S, Wang L, *et al*. Inhibition of tumor propellant glutathione peroxidase 4 induces ferroptosis in cancer cells and enhances anticancer effect of cisplatin. *J Cell Physiol.* 2020;235(4):3425–3437. doi: 10.1002/jcp.29232

[18] Jo A, Bae JH, Yoon YJ, *et al*. Plasma-activated medium induces ferroptosis by depleting FSP1 in human lung cancer cells. *Cell Death Dis.* 2022;13(3):212. doi: 10.1038/s41419-022-04660-9

[19] Lee C. Western blotting. *Methods Mol Biol.* 2007;362:391–399. doi: 10.1007/978-1-59745-257-1_30

[20] Nautiyal J, Kanwar SS, Yu Y, Majumdar AP. Combination of dasatinib and curcumin eliminates chemo-resistant colon cancer cells. *J Mol Signal.* 2011;6:7. doi: 10.1186/1750-2187-6-7

[21] Li FJ, Long HZ, Zhou ZW, Luo HY, Xu SG, Gao LC. System X_c^-/GSH/GPX4 *axis*: An important antioxidant system for the ferroptosis in drug-resistant solid tumor therapy. *Front Pharmacol.* 2022;13:910292. doi: 10.3389/fphar.2022.910292

[22] Chen H, Wang C, Liu Z, *et al*. Ferroptosis and Its Multifaceted Role in Cancer: Mechanisms and Therapeutic Approach.

Antioxidants (Basel). 2022;11(8):1504. doi: 10.3390/antiox11081504

[23] Mao C, Liu X, Zhang Y, *et al*. DHODH-mediated ferroptosis defence is a targetable vulnerability in cancer. *Nature*. 2021;593(7860):586–590. doi: 10.1038/s41586-021-03539-7

[24] Xu T, Ding W, Ji X, *et al*. Molecular mechanisms of ferroptosis and its role in cancer therapy. *J Cell Mol Med.* 2019;23(8):4900–4912. doi: 10.1111/jcmm.14511

[25] Miotto G, Rossetto M, Di Paolo ML, *et al*. Insight into the mechanism of ferroptosis inhibition by ferrostatin-1. *Redox Biol.* 2020;28:101328. doi: 10.1016/j.redox.2019.101328